2017 IEEE/RSJ International Conference on Intelligent Robots and Systems (IROS)
September 24–28, 2017, Vancouver, BC, Canada

GOAT: A Legged Robot with 3D Agility and Virtual Compliance

Simon Kalouche

***Abstract*— Today's cutting-edge in dynamic legged robots use leg topologies which enable agile behaviors such as running and jumping but most of these dynamic behaviors occur primarily in the robot's sagittal plane. Navigating complex environments, however, requires the use of omni-directional dynamic maneuvers for traversing obstacles in confined spaces. This paper introduces GOAT, the Gearless Omni-directional Acceleration-vectoring Topology — a novel 3-DoF, 3-RSR leg topology combined with a direct-drive or quasi-direct-drive (QDD) actuation scheme to enable high fidelity proprioceptive force control and multi-modal mobility via high-energy, omni-directional jumping, running, and walking. GOAT's kinematics, mechanical design, actuation, drive electronics, and control algorithms are presented. Experimental results successfully demonstrate a mechanically robust GOAT leg performing a) explosive vertical jumping up to 82 cm b) landing using high fidelity virtual compliance and c) high-speed omni-directional running/jumping trajectories while mounted on a test rig.**

I. Introduction

It is estimated that nearly 50% of Earth's landmass is currently inaccessible to wheeled or tracked machines [2]. Humans and animals, however, are readily able to access most of these areas and it is desirable that robots and machines be able to do the same. Biologically inspired robots, specifically legged robots, offer enhanced mobility in these impassable environments in situations where it is unsafe or unfeasible for humans to travel. Although there exist dozens of promising legged robots today, most are limited dynamically and all make significant trade-offs between efficiency, dexterity, and dynamic mobility [5]-[11]. Thus, there are still open questions pertaining to leg topology and actuation schemes which best optimizes performance across the efficiency, dexterity, and dynamic mobility spectrum.

Although legged robots utilize a variety of leg topologies, today's most prominent, dynamic legged robots (SpotMini [1], MIT Cheetah [6], ATRIAS [7], Minitaur [9], etc.) share a fundamental shortcoming that constrains the leg's most powerful actuators, force producing capability, and thus dynamic mobility, to the robot's sagittal plane. Sagittally constrained or 2.5D dynamic motions severely inhibit a robot's mobility in real-world 3D environments.

For effective high-speed traversal through complex, unmapped and unstructured 3D environments a legged robot should 1) have an omni-directional leg Jacobian and 2) be able to efficiently deliver and absorb energy from jumping and landing for purposes of both energy efficiency and mechanical robustness. To address the second requirement many researcher's have recently designed robot's with built-in, mechanical compliance using pneumatics, series-elasticity, leaf springs, or bow-legs [2][7][13]. Alternatively, high fidelity virtual model control (VMC) can adequately deliver and absorb high energy in a controllable manner. VMC uses motors to emulate the dynamics of mechanical components such as springs and dampers [16]. VMC also affords the robot the ability to tune leg stiffness and dampening, in real-time, to be optimal for changing terrains and running speeds.

[1]S. Kalouche is with Stanford University's AI Lab and Carnegie Mellon's Robotics Institute, USA. {kalouche@cs.stanford.edu}

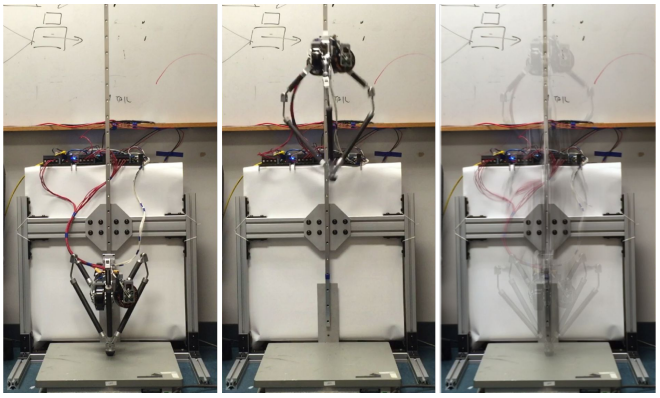

Fig. 1. High jump experiments with the GOAT leg delivering 20.11 J of energy to produce a maximum jump height of 82 cm which is more than double the body height. For full video see [4]

II. Leg Design Principles for Agility

Common design requirements for high energy transfer and agility in legged robots include:

1) **High force, high speed legs:** high torque density actuators; low leg mass/inertia; high energy delivery
2) **Passive/Active Compliance:** Accurate high bandwidth force control; low mechanical impedance; variable leg impedance
3) **Resilient leg mechanics:** High specific strength materials
4) **Energy efficient system:** eliminate sources of loss; energy regeneration or elastic energy storage

For passive compliance using SEAs can be desirable for protecting the transmission and passively conforming to unmodeled disturbances [15]. In SEAs, however, the series-spring acts as a second order mechanical low-pass filter on high frequency dynamics which imposes an upper limit on actuation bandwidth needed to produce and transfer force rapidly. SEAs also fix a single mechanical spring/dampening coefficients to the leg and introduce control complexities associated with modeling spring compliance. The series-spring's stiffness determines the actuation bandwidth for force and position trajectories. The bandwidth and impact force of a simple SEA is calculated as a function of the transmission's reduction ratio n, the spring stiffness k_s, and the motor's rotor inertia I_m using eqs. 1 and 2, respectively.

$$\omega_n = B = \sqrt{\frac{k_s}{n^2 I_m}} \tag{1}$$

$$F_{impact} = \sqrt{(k_s + k_g) n^2 I_m} \tag{2}$$

where k_g is the environment stiffness of the contact point [12].

To avoid the actuation bandwidth limitations of SEAs, VMC using direct-drive or quasi-direct-drive actuators can be used. High fidelity proprioceptive force control is necessary for effectively producing virtual leg compliance upon impacts and it can also be a very high-bandwidth indicator of gait state transitions (i.e. flight to stance phase). Friction, stiction, backlash and reflected inertia in transmissions increase an actuator's mechanical impedance

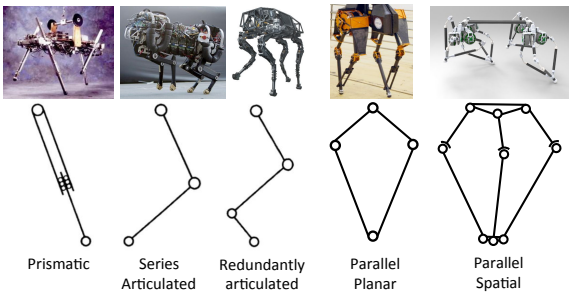

Fig. 2. Common robot leg topologies. The robots shown from left to right include the Raibert quadruped [2], MIT Cheetah [6], Boston Dynamics Big Dog [5], ATRIAS [7], the 3-RSR GOAT leg.

and decrease total system bandwidth [12]. In order to track and command faster force trajectories, the closed-loop bandwidth must be increased by both the actuator and leg mechanics. Therefore, a high transparency and highly backdrivable actuator — where all force at the output can be sensed at the input — is optimal for high fidelity and thus high bandwidth proprioceptive force control [12]. The effect of the transmission ratio n and its corresponding reflected inertia on system bandwidth is theoretically quantified using equations 1-2 where $k_s = 10^6\ Nm$ is the series stiffness of a stiff gear train without an elastic element.

Torque Density, Force Transparency, and Efficiency

Direct-drive and *quasi* direct-drive actuation offers several benefits as compared to geared or series-elastic counterparts. These benefits include high force transparency (low impedance), mechanical robustness to large impacts, and high force control bandwidth. Using direct-drive actuators also presents a few disadvantages which include drastically lower thermal specific torques and lower operating efficiencies during high torque motions [17].

While augmenting an actuator with a gearbox can increase the actuator's torque density by orders of magnitude it does so at the cost of added control complexities, increased reflected inertia, efficiency losses and reduced mechanical robustness [17]. Control complexities are derived from the difficulty in modeling the non-linearities associated with backlash, coulomb and viscous friction, and stiction in the gear train– all of which hinder current-based torque sensing. These non-linear effects 'hide' forces acting at the output from being sensed by the motor causing motor current to be a poor indicator of output torque.

For direct-drive actuators to generate sufficient torque in legged robots the motors must operate in the high torque, low speed regime. However, electromagnetic motors have peak electrical to mechanical power conversion efficiency in the low torque, high speed regime (near the no load speed). Therefore, the production of high torques at low speed requires high current as torque is directly proportional to motor current ($\tau = k_t i$). Joule heating expressed as, I^2R, is the dominant source of energy loss in this operating regime. Therefore, by using a single stage reduction (planetary or friction drive) the motor can produce the same torques using a fraction of the current thereby reducing Joule heating losses. To this end, we argue for energy efficiency purposes that a savings of $\mu I^2 R$ power, where μ is the percent decrease in current, I, required to produce a given torque, is worth the $\approx 3\%$ transmission losses and the nearly-negligible added control complexity of a single stage planetary gear train. An actuator characterization and comparison was performed using a T-Motor U10 alone (DD), a T-motor U10 augmented with a Matex 1:7 single-stage planetary reduction (QDD) where the bandwidth and proprioceptive force sensing accuracy of the QDD was

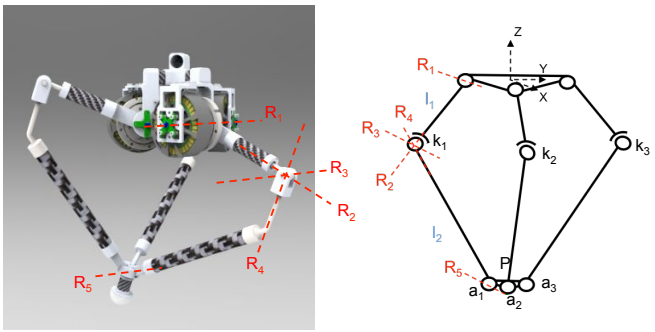

Fig. 3. the 3-RSR leg topology decomposed into the individual joints at the hip R_1, knee R_2,R_3,R_4, and ankle R_5.

40 Hz and 0.4 Nm, respectively as compared to that of the direct-drive actuator which achieved a bandwidth and proprioceptive force sensing accuracy of 70 Hz and 0.15 Nm.

III. GOAT'S 3-RSR LEG TOPOLOGY

To address the current limitations in sagitally constrained, *2.5D* dynamic robots, the GOAT leg is synthesized to have an omni-directional leg Jacobian capable of vectoring large forces at high speeds along any direction in the robot's frontal plane. The 3-RSR topology (schematic shown in Fig. 3 is a 3-DOF parallel mechanism which uses coupled actuation to distribute foot loads over three actuators, thus increasing leg thrust for dynamic jumping and reducing individual actuator effort, size, and mass. This is in contrast to the other leg topologies which have decoupled actuators relying on a single actuator for producing sagittal plane thrust forces and another actuator for producing dorsal plane forces.

To avoid the complexity in determining a closed form analytical solution, the 3-RSR's forward and inverse kinematics are solved using MATLAB's *lsqnonlin()* function and mexxed to C++ for real time constrained optimization. Nine constraint equations construct the cost function for the forward and inverse kinematics optimization. A binary term in the cost function constrains the z-component of foot plate normal to be negative. For the forward kinematics each knee position k_i is known as a function of θ, the actuated joint R_1 at the hip from Fig. 3. The constraint eqs. used to solved the kinematics are expressed below (where $j = i + 1$ is used for more concise notation)

$$0 = w_1\Big((a_{x,i} - k_{x,i})^2 + (a_{y,i} - k_{y,i})^2 + (a_{z,i} - k_{z,i})^2 - l_2^2\Big)$$
$$0 = w_2\Big((a_{x,i} - a_{x,j})^2 + (a_{y,i} - a_{y,j})^2 + (a_{z,i} - a_{z,j})^2 - f^2\Big)$$
$$0 = w_3\Big(\mathbf{n}_b \cdot \mathbf{n}_{k,i}\Big)$$
$$\mathbf{n}_b = \frac{(\mathbf{a}_1 - \mathbf{a}_2) \times (\mathbf{a}_2 - \mathbf{a}_3)}{||(\mathbf{a}_1 - \mathbf{a}_2) \times (\mathbf{a}_2 - \mathbf{a}_3)||}$$
$$\mathbf{n}_{k,i} = \frac{(\mathbf{k}_i - \mathbf{a}_i) \times (\mathbf{a}_i - \mathbf{P})}{||(\mathbf{k}_i - \mathbf{a}_i) \times (\mathbf{a}_i - \mathbf{P})||}$$

where, $i = 1, 2, 3$ represents each chain of the 3-RSR, w_i is the weight for each constraint in the cost function, $\mathbf{P}$ is the $[x, y, z]^T$ position of the foot center, $\mathbf{a}_i$ is the $[x, y, z]^T$ position of each chain's 'ankle' revolute (R-joint), f is the fixed perpendicular distance between each ankle R-joint, and $\mathbf{k}_i$ represents the $[x, y, z]^T$ position of each chain's spherical 'knee' joint calculated by

$$\mathbf{k}_i = \mathbf{h}_i * \mathbf{T_{h2k}} = [\mathbf{R}_{R_1}(\theta_i), l_1]$$

In Fig. 3 The 'ankle' joints are the 3 R-joints (denoted R_5) at the distal foot plate, the 'knee' joints is the point where R_2, R_3,

and R_4 intersect, and the hip joints are attached to the top hip plate and denoted by R_1.

Like the forward and inverse kinematics the Jacobian is solved numerically by differentiating the forward kinematics transformation matrix with $\epsilon = 10^{-6}$ for adequate numerical accuracy. For the 3-RSR leg, the Jacobian is a 6 by 3 matrix[1] The Jacobian is constructed as follows

$$\mathbf{J}_{6\times3}(\boldsymbol{\theta}) = \begin{bmatrix}\mathbf{T}_{3\times3}\\ \boldsymbol{\Omega}_{3\times3}\end{bmatrix}$$

$$\mathbf{T}_{3\times3} = \frac{1}{\epsilon}\Big[\mathbf{b}_{t,1}-\mathbf{a}_{t,1}, \mathbf{b}_{t,2}-\mathbf{a}_{t,2}, \mathbf{b}_{t,3}-\mathbf{a}_{t,3}\Big]$$

$$\boldsymbol{\Omega}_{3\times3} = \frac{\mathbf{A}_{R,i}}{2\epsilon}\Big[\mathbf{W}_{32}-\mathbf{W}_{23}, \mathbf{W}_{13}-\mathbf{W}_{31}, \mathbf{W}_{21}-\mathbf{W}_{12}\Big]^T$$

where $\mathbf{W} = \mathbf{A}_R^T\mathbf{B}_R$ and $\mathbf{B}_i = \mathbf{T}_{h2f}(\boldsymbol{\theta}+\epsilon) = [\mathbf{B}_{R,i}, \mathbf{b}_{t,i}]$, $\mathbf{A}_i = \mathbf{T}_{h2f}(\boldsymbol{\theta}) = [\mathbf{A}_{R,i}, \mathbf{a}_{t,i}]$ are transformations from the hip to the foot $\mathbf{T}_{h2f}$, for chain i, with input hip angles $\theta+\epsilon$ and θ, respectively.

IV. Comparison of 3-DoF Leg Topologies

In Figs. 4-6 and Table I the 3-RSR GOAT leg is compared against conventional series-articulated leg designs (MIT Cheetah, StarlETH, SpotMini) and prismatic legs (Raibert Hopper) in end-effector workspace and force envelope.

Four measures of legged 3D agility are defined and listed in Table I as the energy delivered by leg thrust (E); the force envelope volume (Ψ) which describes how much force can be exerted over the limb's workspace; the foot force to leg mass ratio, or limb acceleration (Λ); and the proprioceptive force sensitivity (Π) which is a metric of the minimal joint torque resolution required to measure a change in foot force f to $f+\epsilon$ at foot position i within the limbs workspace, where ϵ is arbitrarily small (1 N in this study). These measures are normalized by assuming all leg topologies have

[1]the size of the Jacobian is 6 by 3 because the force-torque wrench is a 6x1 vector and the number of driven actuators is 3 or a 1x3 vector.

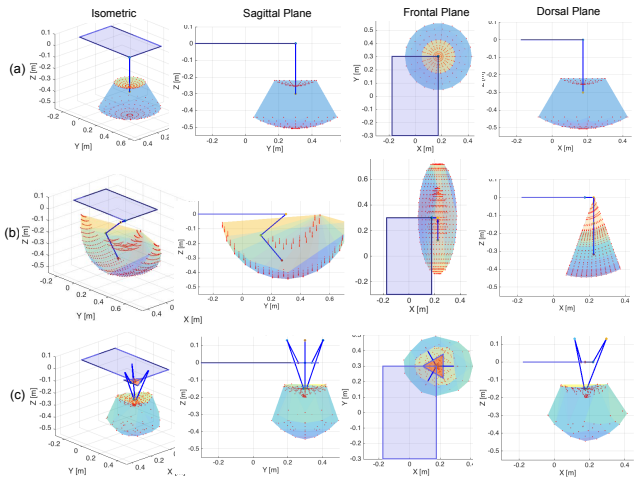

Fig. 4. Workspace volume for the (a) prismatic, (b) series-articulated, & (c) 3-RSR topologies shown on a quadruped body hiding all but 1 leg. Joint limits used for series-articulated & prismatic legs are based on the joint limits of the MIT Cheetah & the Raibert Hopper.

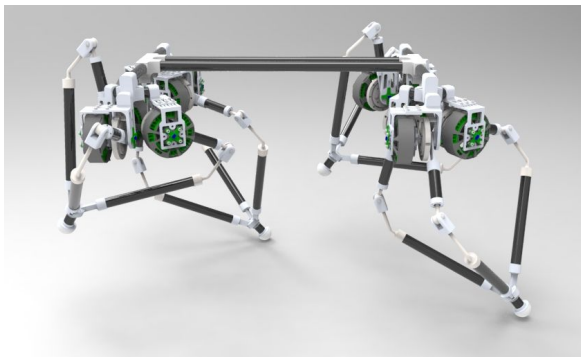

Fig. 5. A viable quadruped using the GOAT 3-RSR leg topology.

an identical set of 3 equally sized and performing actuators.

$$E = F_{avg}\Big(d_{foot}\Big)_{max} \tag{3}$$

$$\Psi = F_{avg}\cdot V_{ws} \tag{4}$$

$$\Lambda = \frac{F_{avg}}{m_l} \tag{5}$$

$$\Pi = \frac{1}{n}\sum_{i=1}^{n}|J_i^T F(f) - J_i^T F(f+\epsilon)| \tag{6}$$

where F_{avg} is the average foot force along a foot trajectory, m_l is the unsprung leg mass, and $(d_{foot})_{max}$ is the maximum distance traveled by the foot along a linearly extending trajectory as shown by example in Fig. 6(c) by the black line. $(d_{foot})_{max}$ is a function of the limbs workspace V_{ws}.

A. Force Envelope Analysis

Figure 6 shows that to produce a force-torque wrench, F_{foot}, as defined in eq. 8 the required joint torques are smaller for the 3-RSR leg than for the other topologies. The plots are generated using a quasi-static force analysis in which joint torques are solved using the Jacobian transpose method

$$\tau_m = J^T F_{foot} \tag{7}$$

$$F_{foot} = f[-\sin\phi\sin\theta, -\sin\phi\cos\theta,\ \cos\phi,\ 0,\ 0,\ 0]^T \tag{8}$$

where $f = -100$ N, $\phi = \tan^{-1}(\frac{step\ length}{step\ height})$, and θ is the direction or heading in the frontal plane ($\theta = 0^o$ points in direction of +Y).

B. Workspace Analysis

Figure 4 shows the available workspace for each of the leg topologies. Although the 3-RSR has a smaller limb workspace than series-articulated legs, this sacrifice is reasonable considering the subset of the entire workspace of legged robots which is actually used in practice to walk, run, or jump is not excessively large and is for the most part contained within the 3-RSR's workspace. Compared to conventional parallel mechanisms the 3-RSR has superior workspace which can be attributed to the dual configuration of the knee joint where each configuration can be smoothly reached without forcing the mechanism to pass through a singularity

C. Proprioceptive Force Sensitivity Analysis

A major theme in the synthesis of the 3-RSR leg was design for simple, high fidelity, virtual model control which would ultimately enable virtual compliance. To achieve such performance an important criteria is the ability to

1) rapidly change actuator torques to emulate the bandwidth of a mechanical spring-damper
2) accurately sense and deliver foot forces using joint torques through the leg Jacobian.

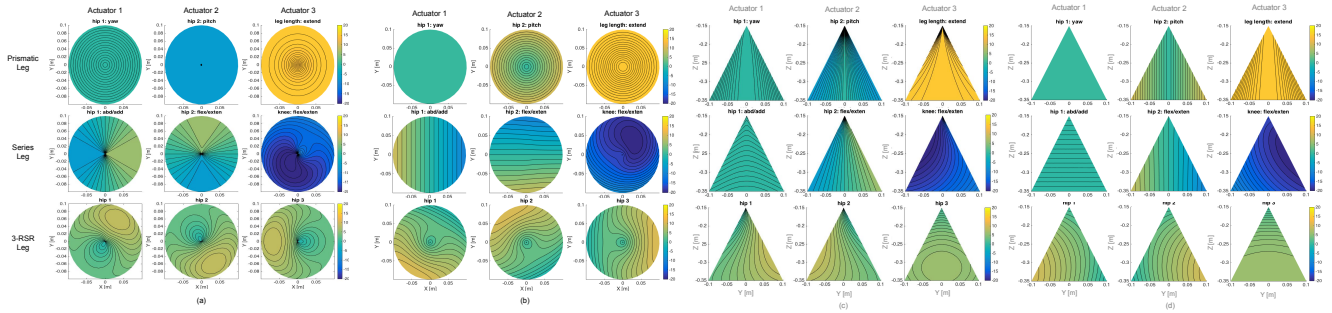

Fig. 6. Frontal (a-b) and sagittal (c-d) plane force envelope of the 3-RSR leg as compared to the series-articulated and prismatic legs. The x and y axes correspond to the coordinates of the foot in the leg frame. The color contour represents the required torque from each actuator to produce the defined force wrench at that foot coordinate in the workspace. In (a,c) the foot force follows eq. 8, while the foot force in (b,d) is always -100 N in the z-direction.

From the second criterion, it is evident that the force transparency of the entire leg system must be maximized to ensure accuracy in forces being sensed and delivered to mimic mechanical compliance at kHz time scales.

Proprioceptive sensing is also dependent strongly on leg topology which determines the Jacobian. Because the transpose of the leg Jacobian relates foot forces and joint torques, an ideal leg topology for accurate proprioceptive sensing will have a leg Jacobian with a high sensitivity in joint torques to changes in foot force. This design insight, in combination with minimizing mechanical impedance is needed to design limbs with adequate proprioceptive force sensitivity for virtual compliance.

Fig. 7 shows — for every foot position in each limb's workspace (prismatic, series-articulated, 3-RSR) — the proprioceptive force sensitivity Π. The contour plot's color represents the value of Π, the minimum torque resolution needed to sense a 1N force change at the foot in the position designated by the (x,y) coordinate of plot 7.

The design of the 3-RSR attempted to balance and optimize many metrics associated with legged agility and proprioceptive force control. Table I provides a summary and comparison of the 3-RSR's performance metrics as compared to the series-articulated and prismatic leg topologies.

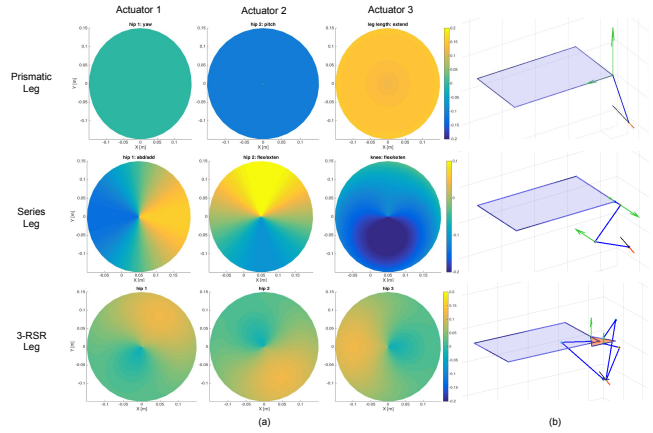

Fig. 7. (a) Top view of frontal plane for each leg topology. The contour plot indicates by color what the proprioceptive sensitivity (i.e. torque in N-m) of each actuator is to a 1 N force acting on the foot. The coordinate on the plot corresponds to the {x,y} position of the foot. (b) shows a simulation of the legs producing a force vectored in the direction indicated by the orange arrow. The green arrows indicate relative magnitude of the 3 actuator torques required to produce the desired foot force.

V. Mechanical Design of the 3-RSR

The 3-RSR is mechanically constructed of a hip plate, foot plate and 3 identical legs consisting of two links that connect the hip to the foot. The kinematic configuration of the leg is shown in Fig. 3 where the physical realization of the mechanism is a 3-R-RRR-R or 3-5R, where each R-joint denotes a 1-DoF revolute joint. The three motors are coupled directly to their corresponding first link or through a single stage planetary transmission in the case of QDD actuation. The motor stator is bolted to the hip structure which is adjustable to accommodate different actuator configurations (DD or QDD). Link 1 (l_1) is double supported by bearings on each side to increase moment loading capacity. l_1 has one rotational degree of freedom about revolute joint axis 1 (R_1) in Fig. 3 where the axes of the three hip joints are parallel to the hip plane but phased 120^o apart to evenly space the 3 legs of the 3-RSR.

The knee joint consists of three, 1-DOF revolute joints whose rotation axis intersect at one point as shown in Fig 8. This configuration achieves the mobility of a spherical joint where the range of motion for joints R_2 and R_4 is 360^o while the range for R_3 is $\pm 90^o$. The extended range of motion of the RRR joint allows for the leg to pass through its two configurations: knee-above-hip and knee-below-hip as shown in Fig. 1.

To minimize the mechanical impedance of the leg mechanism with force transparency in mind, a large effort was made to reduce and eliminate all sources of friction. Therefore bearings rated to

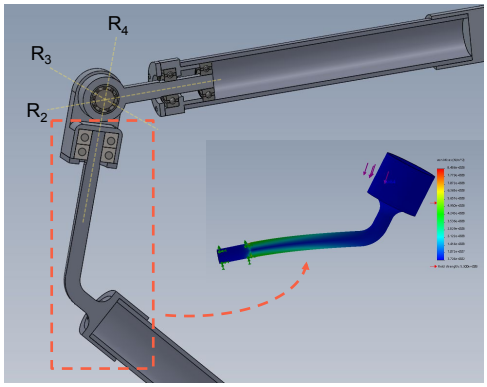

Fig. 8. Knee joint design showing the 3 revolute joints with intersecting axes. Solidworks FEA results indicate that stresses as high as 123 ksi are present at the bearing support shaft of the distal knee segment with a conservative applied force of 300 N and safety factor of 4. Therefore, this component is machined from medium carbon steel with 125 ksi yield strength in contrast to most of the other components which are machined from 7075 Aluminum with 73 ksi yield strength.

TABLE I

COMPARISON OF PERFORMANCE MEASURES FOR 3-DOF LEG TOPOLOGIES.

Topology	**Max Actuator Torque** [N-m]			**Work Space**	**Leg Volume**	**Foot Force**	**Foot Speed**	**Limb Inertia**	**E**	**Ψ**	**Λ**	**Π**
	1	2	3	[m^3]	[m^3]	[N]	[m/s]	[kg-m^2]	[J]	[N-m^3]	[m/s^2]	[N-m]
Prismatic	0.6	9.1	15.0	.0283	.0006	33.3	2.82	0.111	6.7	.94	37	0.0226
Series	11.2	6.7	22.5	.0395	.0030	36.4	9.65	0.058	7.3	1.44	79	0.0667
3-RSR	9.5	9.5	9.5	.0285	.0171	131.5	2.65	0.015	27.0	3.75	209	0.0506

Note: Max Actuator Torque refers to the maximum torque required to produce the wrench in eq. 8 at every point in a vertical foot trajectory. Leg Volume is the worst-case. Foot Forces and Velocities are the average over a vertical leg trajectory. The prismatic leg uses a rotary to linear mechanism with a reduction of 1:6.7. **Ψ** is the value of the workspace volume multiplied by the average foot force in that workspace.

handle large radial and moment loads were used at each of the 15 joints in the 3-RSR leg.

The sole of the foot is made of molded urethane rubber from SmoothOn. The rubber acts as a mechanical damper and shock absorber to filter out very high frequency (> 500 Hz $\approx \omega_n$ the natural frequency of the rubber foot) impulse forces during landing.

Motor selection to drive the QDD or DD actuator was based on maximizing thermal specific torque. It was determined in [9] that the T-motor U8, and more generally the U-Power Series, had superior torque density as compared to other commercial off-the-shelf (COTS) motors.

To increase the torque density of the GOAT leg's actuators, a single stage gear stage can be placed between the motor and the drive hip link. In [3] it was shown that adding a single stage planetary would decrease energy requirements for generating a desired torque by allowing the motor to operate in a more efficient regime with lower current and thus lower Joule heating losses and less saturation from thermal management or RMS limiting while mitigating many of the common negative effects of geared transmissions. The QDD was shown to maintain a bandwidth of 40 Hz and proprioceptive torque sensing within 6% error [3].

VI. ELECTRICAL DESIGN

Three PCBs are used to drive and communicate with the actuator module. The motor driver board is based off a TI Piccolo TMS320F28069M MCU and a DRV8301 Bridge Driver. This board runs the low level field-oriented control (FOC) motor commutation (at 25 kHz) and PID controllers for separate position, velocity, and torque control (at 10 kHz). A separate PCB holding an AMS AS5048A magnetic encoder senses the change in magnetic field from a rotating diametrically polarized magnet fixed to the rotor axle. The third custom board is a Hebi prototyping I/O board with various input/output channels including SPI, I2C, Serial, and Ethernet which handles high level communications. The power electronics are capable of energy regeneration to convert work done on the leg back into battery potential for added efficiency.

To maximize performance yield from the T-motor an RMS current monitor overdrives and saturates the current output commanded to the motor if the RMS value exceed the continuous rated current. This keeps the motor within its calibrated thermal limits while allowing short instances of multiple times the rated continuous current.

VII. EXPERIMENTS

For preliminary testing the GOAT leg is constrained to a 1-DoF vertical test rig using a 15.5 mm wide linear bearing and guide rail shown in Fig. 1. All electronics and power are mounted off-board currently, although custom electronics are currently being developed for on-board mounting. The electronics and battery are expected to add a mass of 1 kg (0.75 kg for battery and 0.25 kg/leg for electronics).

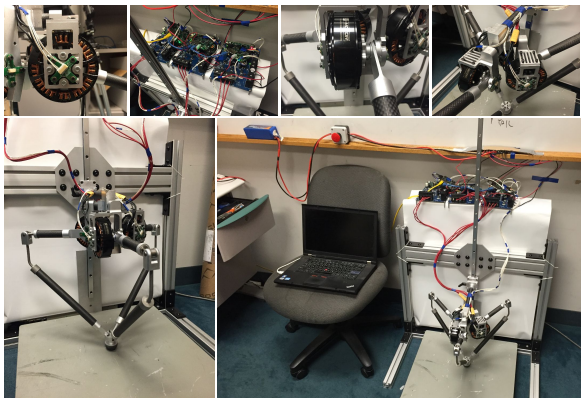

Fig. 9. GOAT Leg prototype and experimental 1-DoF vertical jumping test bed. The robot hops on a 6-axis force-torque load cell.

The full leg mechanism was tested to determine the mechanical friction present in the system. Equal joint torques were commanded at each of the three hip actuators starting at zero and increasing until motion in the leg was seen. The torque at each actuator was found to be around 0.063 N-m when the leg began to to move. This is compared to the static friction in each motor of around 0.048 N-m indicating minimal added friction in the actual mechanism.

A. Omni-Directional Force Vectoring with Force Plate

In section IV the 3-RSR topology was theoretically shown to be superior in terms of requiring the least amount of joint torque per actuator to generate omni-directional force-torque wrenches. To experimentally validate the 3-RSR's ability to deliver omni-directional force equally along all vectors a test which commanded the leg to generate 18 force-torque wrenches defined by eq. 8 where θ ranged from 0 to 360 in increments of 20 degrees was conducted while on a 1-DoF test rig. The resulting data collected by a 6-axis AMTI OR6-7-2000 force-torque plate show that the magnitude of force produced in the x direction is equal to the magnitude of foot force produce in the y direction verifying analytical results which indicate omni-directional frontal plane force vectoring equality.

B. Omni-Directional Running

To test omni-directional running and walking ability, the GOAT leg was fixed on a 1-DoF test rig so that the foot could not touch the ground. The foot was then commanded through a minimum jerk spline trajectory for omni-directional running. The leg was able to reach high running speeds with a stride length of 0.25 m at 2.4 Hz. A video showing seamless changes in running direction

as well as high speed running trajectories can be found here: https://www.youtube.com/watch?v=n319xVomJTQ.

VIII. Summary and Design Insights

This section highlights and summarizes the key design insights and advantages that the novel 3-RSR GOAT leg offers with respect to other, more common, leg topologies. The GOAT leg

1) seems to be mechanically robust to large 3D forces and even large falls. The leg was never broken during any of the high jumping, landing, and hopping tests.
2) analytically and experimentally demonstrated generation of omni-directional force-torque wrenches at the foot with less required torque per actuator than the other leg topologies.
3) requires less torque per actuator and distributes foot loads over multiple actuators enabling the use of DD and QDD actuation to achieve both explosive power and high fidelity proprioceptive force sensing for virtual compliance.
4) has optimized leg parameters which increase its workspace to encompass most of the required workspace for legged locomotion including walking, running, and jumping.
5) has very low limb inertia as compared to all current legs as all the actuators' stators are static and fixed to the hip frame. This means that the mass of the actuators does not contribute to the inertia of the leg like in the MIT Cheetah and other serially configured designs.

The GOAT leg has proven itself to be a mechanically robust 3D parallel mechanism with 3 degrees of freedom which allow it to exert force equally along any vector in the frontal plane with less required torque than would be required by the prismatic, series articulated, and parallel planar topologies. While series-articulated limbs can use one large actuator at the knee for sagittal plane jumping and tilt the entire leg to produce out-of-plane forces, the leg structure is, similarly, not designed to bear high lateral forces. Additionally, for the series-articulated and prismatic limbs to produce forces at vectors which do not pass directly through the hip joint, much larger torques from the hip abduction/adduction actuator as well as the hip flexion/extension actuators are required. Therefore, if these actuators are made small — assuming the knee actuator will bear the brunt of the loads required for jumping — then the prismatic and series articulated leg topologies would be much weaker in producing omni-directional force vectors at any spot within their workspace as compared to the 3-RSR GOAT leg.

Also, by relying on a single actuator to carry the load for jumping as done in the prismatic and series-articulated limbs, that actuator must almost certainly be outfitted with a transmission to produce required torques/forces. This comes at the sacrifice of an unequally distributed proprioceptive force sensitivity from each actuator. Therefore, it is important to note that a parallel leg topology which distributes foot loads over multiple actuators does not need to sacrifice proprioceptive sensing accuracy (by adding a transmission) for agility.

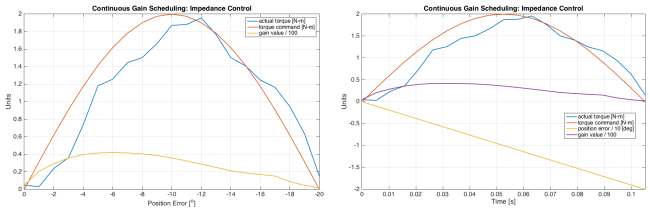

Fig. 10. Experimental results using impedance controller based on continuous gain scheduling. The position error increases linearly with time but the commanded torque trajectory is non-linear (sinusoidal). Any arbitrary torque trajectory can be chosen; the continuous gain scheduler will modulate the gain based on the desired torque and the current position error. The torque trajectory is followed within 10% error by the direct-drive actuator at a bandwidth greater than 200 Hz.

IX. VMC for Compliant Dynamic Motions

The use of virtual model control for compliant monopod hopping allows virtual spring and damper components to be created using high bandwidth motors with accurate proprioceptive torque sensing to mimic the forces produced by mechanical spring and dampers. Virtual full leg compliance is accomplished by servoing the torque of each joint actuator — using the Jacobian transpose method — at kHz timescales to produce foot forces which would match the force applied on the body if a physical **prismatic-spring connected the hip to the foot**. Implementing virtual spring and dampers can be done by specifying a time-varying force-torque wrench as a function of nominal foot position and foot velocity as follows.

$$F = [f_x \quad f_y \quad f_z \quad 0 \quad 0 \quad 0]^T \tag{9}$$

$$f_z = k_s(z_{fbk} - z_{cmd}) + k_d(\dot{z}_{fbk} - \dot{z}_{cmd}) \tag{10}$$

where f_z is the vertical component of the force torque wrench to be applied by the leg emulating a virtual spring-damper (f_x and f_y are calculated similarly), k_s is the virtual spring stiffness [N/m], k_d is the virtual dampening coefficient [N-s/m], and z is the z-coordinate of the foot position where the subscripts z_{cmd} and z_{fbk} denote the commanded and feedback positions. Typically $\dot{z}_{cmd}$, the commanded foot velocity in the z-direction, is set to zero. Once the virtual spring force-torque wrench F is determined with any desired spring and dampening coefficients (within the motors capabilities) the joint torques (τ) needed to produce this virtual force at any instant in time can be calculated using the Jacobian transpose $\tau = J^T F$.

A. Experimental Validation

1) Control for Virtual Spring-Damper Leg: The control architecture for the 1-DoF hopping controller which uses virtual model control to virtually emulate a mechanical spring/damper is shown in Fig. 11. This controller allows the leg to compliantly absorb the impact during touchdown/landing, while providing large leg thrust forces for exerting large amounts of energy required for high jumping. The controller has a **Flight** and **Stance** phase of which the stance phase is composed of two sub-states: 1) stance and 2) jump.

2) Impedance Control Using Continuous Gain Scheduling: To achieve high-fidelity virtual compliance a modified impedance controller was implemented which modulates position gains rather than joint position to generate a desired torque trajectory to emulate a desired arbitrary linear or non-linear spring. The components of the impedance control scheme are shown within the dotted box in the controller flow diagram in Fig. 11.

With a user-defined spring stiffness and dampening profile a virtual spring-damper foot force is determined at time t depending on the foot position relative to the user-define 'nominal' foot position (i.e. position where the spring leg is not virtually compressed), the Jacobian is used to transform that virtual spring-damper foot force into joint torques at the 3-RSR's 3 hip joints. These 3 joint torques becomes the desired torque command at the current time step. The desired joint torques τ are then fed, along with the joint position error ($pos_{err} = pos_{fbk} - pos_{cmd}$), to the impedance controller. The impedance controller then interpolates between the calibrated family of position error vs torque curves (shown in Fig. 12) for various position gains to determine the continuous gain value which

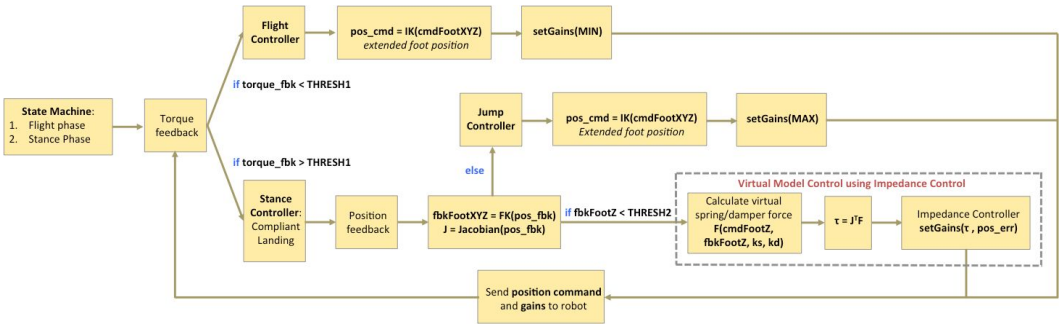

Fig. 11. Schematic of the hopping control architecture using virtual model control to virtually emulate a mechanical spring/damper.

will generate the desired torque at the current position error [3]. This gain value is modulated and assigned at a frequency of 1 kHz which enables the leg to mimic the response of a virtual spring damper at a very high bandwidth. High bandwidth torque tracking through this modified impedance controller is shown in Fig. 10.

The controller then operates in a finite state machine triggered by internally sensed gait transitions. A jump is initiated by extending the leg using very high position gains. Once a land occurs and the state machine is switch to stance phase, the virtual model impedance controller operates and modulates hip torques to produce effective whole leg compliance which mimics a mechanical spring between the hip and the foot. This controller operates until the foot position or virtual spring is compressed passed a certain threshold in which the jump controller is called in the case of continuous hopping. This allows the energy transfer of the landing rebound to aid the motors in generating leg lift-off thrust to jump again. Once a jump occurs, the process repeats to produce cyclic hopping with a stable apex hopping height.

B. Virtual Compliance Experiments

Using the continuous gain scheduling impedance controller, precise torques could be generated at the hip joint at over 200 Hz enabling high fidelity virtual model control. Numerous tests were conducted using various virtual spring and dampers. Virtual compliance was tested at the joint level as joint compliance — emulating the use of physical torsion springs at hip — and as full leg compliance — emulating the use of a physical spring-damper connecting the hip to the foot.

The results for three such tests using virtual joint and full leg compliance are shown in Fig. 13. The two top rows correspond to torsional joint springs with stiffness of 18 and 36 Nm/rad,

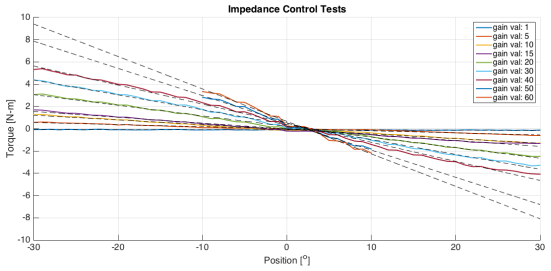

Fig. 12. The impedance controller generates the desired joint torque indirectly by interpolating this family of calibrated position-error vs. torque curves and setting motor gains to the value of the curve which generates the desired motor torque at the current position-error. For example, if the appropriate foot force at time t requires hip joint 1 to have a torque of 4 N-m and the position-error (i.e. deflection of the virtual spring) is 20^o at hip joint 1, then the motor at hip joint 1 will be set to have a gain of 40.

respectively, while the bottom plot has a full leg virtual stiffness of 250 N/m and dampening of 10 N-s/m. The full leg compliance uses a rectified virtual linear spring-damper in which the spring can only exert forces in the negative z-direction. This rectified spring is used to achieve shorter settling times and lower percent overshoot which is normally handled by increasing the virtual damper force. The response for the whole leg compliance with rectified spring-damper force is shown to be ideal as the settling time is the shortest at 0.17 seconds compared to the settling times of the joint compliance ($>$ 2 seconds). In these tests the two performance results desired were minimized settling time and minimized overshoot.

C. Vertical Agility Experiments

Several high jump experiments were conducted to determine the maximum jumping height for the leg. Within the preliminary tests a maximum jumping height of 82 cm was attained. The robot was able to land compliantly from all jump heights indicating that joint torques required for landing were not the limiting factor. The experimental energy delivered $E_d = mgh_{peak}$ during the highest jump was found to be 20.11 J.

D. 1-DoF Vertical Hopping

Hopping tests were also included in the preliminary experiments. The hopping control framework described in Fig. 11 is used to deliver leg thrusts during take-off and operate using a continuous gain scheduling impedance controller during landing to absorb impacts smoothly using virtual compliance. The supplemental video shows 30 cm hopping at 1.5 Hz on a 1-DoF test rig. The leg was commanded to have a virtual whole leg compliance emulating a rectified prismatic spring with a stiffness of 375 N/m and dampening of 0 N-s/m.

X. Conclusion

This study introduces GOAT, the **g**earless **o**mni-directional **a**cceleration-vectoring **t**opology. GOAT is a novel 3-DOF, parallel 3-RSR leg topology with an optimized workspace driven by an ultra low-impedance actuation scheme for precisely 'feeling' forces and dynamically reacting to the full 3D world around it. This 3-RSR topology expands the multi-modal mobility of dynamic legged robots beyond operating dynamically in the sagittal plane by enabling explosive omni-directional jumping, running, and dexterous crawling. The 3-RSR topology puts all 3 of its actuators in parallel to reduce torque requirements on any one actuator which allows the DD/QDD actuation scheme — which simplify the implementation of high fidelity virtual model control — to be used.

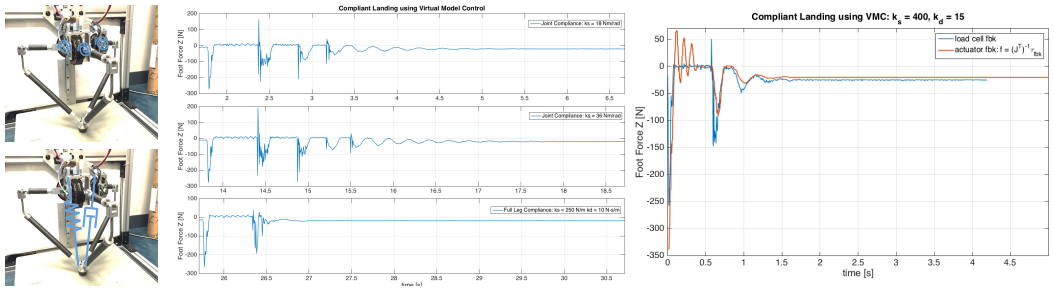

(a) (b) (c)

Fig. 13. a) Virtual joint compliance (top), and virtual full-leg compliance (bottom). b) Experiments using 3 different virtual spring stiffness' and dampening coefficients and observing the response upon landing. The top two plots have virtual joint compliance with stiffness of 18 and 36 Nm/rad while the bottom plot has a full leg virtual rectified spring stiffness of 250 N/m and dampening of 10 N-s/m. c) The average error between the ground truth force-plate foot-force data and the estimated foot-force using proprioceptive torque sensing through motor currents and the leg Jacobian was 16%. The low error indicates the quality of the force transparency of the combined actuators and leg mechanism.

TABLE II

AGILE PERFORMANCE COMPARISON IN DYNAMIC LEGGED ROBOTS. THE BULK OF THE DATA FROM THIS TABLE HAS BEEN TABULATED AND PRESENTED ORIGINALLY BY KENNEALLY ET. AL IN [9]. DOF IS THE DEGREES OF FREEDOM PER LEG.

Robot	Legs #	DoF #	Leg Length $[m]$	Mass [kg]	Motor Mass %	Gear Ratio	Max Vertical Jump Height [m]	Energy Delivered [J]
GOAT	1	3	0.26	2.5	48	n/a	0.82	20.11
MIT Cheetah	4	3	0.275	33	24	5.8	0.5	161.9
Minitaur	4	2	0.2	5.0	40	n/a	0.48	23.5
XRL	6	1	0.2	8	11	23	0.425	33.3
Delta Hopper	1	3	0.2	2.0	38	n/a	0.35	6.9
StarlETH	4	3	0.2	23	16	100	0.32	72.2
HRP3La-JSK	2	6	0.6	54	9.2	??	0.27	143
ATRIAS	2	3	0.42	60	11	50	0.11	64.7

ACKNOWLEDGMENT

The author would like to acknowledge significant contributions in motor drive development by Youshuang Ding and assistance from members of the CMU Biorobotics Lab. This project was funded by Professor Howie Choset and an NDSEG Fellowship.

REFERENCES

[1] Boston Dynamics [Online]. Available: bostondynamics.com
[2] M. Raibert, Legged robots that balance. MIT Press, 1986.
[3] S. Kalouche, "Design for 3D Agility and Virtual Compliance Using Proprioceptive Force Control in Dynamic Legged Robots" Masters Thesis, Carnegie Mellon University, August 2016.
[4] "Introducing GOAT: A Legged Robot with 3D Agility and Virtual Compliance." https://www.youtube.com/watch?v=n319xVomJTQ
[5] M. Raibert, K. Blankespoor, G. Nelson, and R. Playter, "Bigdog, the rough- terrain quadruped robot," Proceedings of the 17th International Federation of Automation Control. April 2008.
[6] S. Seok, A. Wang, D. Otten, S. Kim, "Actuator design for high force proprioceptive control in fast legged locomotion," 2012 IEEE/RSJ International Conference on Intelligent Robots and Systems, 2012.
[7] C. Hubicki, J. Grimes, M. Jones, D. Renjewski, A. Sprowitz, A. Abate, And J. Hurst. "ATRIAS: Design and Validation of a Tether-free 3D-capable Spring-Mass Bipedal Robot." The International Journal of Robotics Research. June 10, 2016.
[8] M. Hutter. "StarlETH & Co. – Design and Control of Legged Robots with Compliant Actuation." Doctoral Thesis, ETH, 2013.
[9] G. Kenneally, A. De, D. Koditschek. "Design Principles for a Family of Direct-Drive Legged Robots." IEEE ROBOTICS AND AUTOMATION LETTERS, VOL. 1, NO. 2, JULY 2016.
[10] K. Galloway, G. Haynes, B. Ilhan, A. Johnson, R. Knopf, G. Lynch, B. Plotnick, M. White, and D. Koditschek. "X-RHex: A Highly Mobile Hexapedal Robot for Sensorimotor Tasks."
[11] W. Bosworth, S. Kim, N. Hogan. "The MIT Super Mini Cheetah: A small, low-cost quadrupedal robot for dynamic locomotion." IEEE, SSRR. West Lafayette, Indiana, 2015.
[12] W. Townsend, "The Effect of Transmission Design on Force-Controlled Manipulator Performance." Doctoral Thesis, Massachusetts Institute of Technology, April 1988.
[13] H.B. Brown, G. Zeglin. "The Bow Leg Hooping Robot." Proceedings. IEEE International Conference on Robotics and Automation, 1998.
[14] J. Hurst. "The Role and Implementation of Compliance in Legged Locomotion." Doctoral Thesis, Carnegie Mellon, 2008.
[15] S. Kalouche, D. Rollinson, H. Choset. "Modularity for Maximum Mobility and Manipulation: Control of a Reconfigurable Legged Robot with Series-Elastic Actuators." IEEE (SSRR), 2015, 1-8.
[16] J. Pratt, C.M. Chew, A. Torres, P. Dilworth, G. Pratt. " Virtual Model Control: An Intuitive Approach for Bipedal Locomotion." IJR Research Vol. 20, 2001, pp. 129-143.
[17] H. Asada and K. Youcef-Toumi, Direct-drive robots: theory and practice. MIT press, 1987.
[18] J. M. Duperret, G. D. Kenneally, J. L. Pusey, and D. E. Koditschek. "Towards a Comparative Measure of Legged Agility." Experimental Robotics: The 14th International Symposium on Experimental Robotics, 2016.
[19] G. Kenneally, D. Koditschek. "Leg Design for Energy Management in an Electromechanical Robot." 2015 International Conference on Intelligent Robots and Systems, September, 2015.
[20] J. Grimes. "ATRIAS 1.0 & 2.0 - Enabling Agile Biped Locomotion with a Template-Driven Approach to Robot Design." Masters Thesis, Oregon State University, 2013.
[21] G. Pratt, M. Williamson. "Series elastic actuators." Intelligent Robots and Systems 95.'Human Robot Interaction and Cooperative Robots', Proceedings. IEEE/RSJ International Conference, 1995.
[22] R. Blickhan. "The Spring-Mass Model for Running and Hopping." J. Biomechanics Vol. 22, No 11/12, pp. 1217-1227, 1989.
[23] H., Neville. "Impedance control: An approach to manipulation." American Control Conference, 1984. IEEE, 1984.